Equation of state of hard lenses: A combined virial series and simulation approach

Philipp Marienhagen and Joachim Wagner*
Institut für Chemie, Universität Rostock, 18051 Rostock, Germany

(Received 15 March 2022; accepted 23 May 2022; published 1 July 2022)

We provide highly accurate equation-of-state data for the isotropic phase of hard lenses obtained by means of cluster Monte Carlo simulations. This data is analyzed using a virial approach considering coefficients up to the order eight and Carnahan-Starling type closure relations for the virial series. The comparison with previously investigated systems consisting of hard, oblate ellipsoids of revolution allows insights into the detailed influence of the particle geometry. We propose a generalized Carnahan-Starling approach as a heuristic equation of state for the isotropic phase of hard lenses that in first approximation shows the same dependence on the excess part of the excluded volume as identified for oblate, hard lenses of revolution.

DOI: 10.1103/PhysRevE.106.014101

I. INTRODUCTION

Hard-body many-particle systems have served for more than a century as model systems for the self-organization of molecular matter [1] with impacts on colloidal soft matter [2–5] or granular systems [6] on the meso- or macroscale. Anisometric particles are of particular interest for the understanding of liquid crystals which attracted large scientific interest, both from the viewpoint of fundamental research and, due to manyfold technical applications, from the viewpoint of applied science [7,8].

While the aspect ratio ν, i.e., the ratio of the shortest to longest extent, is the property that essentially influences the phase behavior and equation of state of such systems, numerous studies are dedicated to the influence of the specific shape beyond the aspect ratio [9–11].

A comprehensive description for differently shaped hard particle systems' equations of state depending on their aspect ratio has often been in the focus of scientific work [12–15] with relevance for classical density functional theory [16]. In their seminal work, Isihara and Hadwiger independently showed that the second virial coefficient of convex hard bodies can be described analytically using fundamental geometric measures of the respective geometry [17–19].

Based on the knowledge of second virial coefficients B_2, we have previously reported that reduced higher-order virial coefficients $\tilde{B}_i = B_i/B_2^{i-1}$, where B_i is the virial coefficient of order i of hard, oblate, ellipsoids of revolution and hard lenses, show in first approximation a universal dependence on the excess part of the mutual excluded volume [20,21].

The aim of this contribution is to calculate equation-of-state data for hard lenses as a geometry similar to hard, oblate ellipsoids of revolution, however, exhibiting an equatorial singularity of surface curvature in contrast to ellipsoids. The comparison of hard, oblate ellipsoids of revolution and hard lenses is a suitable choice, since the phase behavior of both geometries is known and contains the same phases [22–24]. In the case of hard lenses metastable glassy phases have also been reported [25,26].

As previously shown for ellipsoids, cluster Monte Carlo simulations as a biased variant of the original Metropolis scheme are the method of choice for the computation of precise equation-of-state data of hard, anisotropic particles in the (N, p, T) ensemble at constant number of particles N, constant pressure p and constant temperature T. Since in the case of hard-body interaction, the potential energy is either infinite for overlaps or zero otherwise, deviations from the ideal-gas behavior are for such systems independent on the temperature and therewith the thermal energy $\beta^{-1} = k_B T$. Hence, the relevant quantity with impact on the real gas behavior is solely the particle number density ϱ and the related volume fraction $\varphi = V_P \varrho$, where V_P denotes the particle volume.

II. THEORETICAL BACKGROUND

In this paper, equation-of-state data of hard lenses is determined in the isobaric-isothermal (N, p, T) ensemble. As previously shown, employing a cluster Monte Carlo (MC) algorithm [27–29] gives access to precise equation-of-state data with comparatively small computational effort. In comparison to classical (N, p, T) MC, the cluster MC approach allows larger volume fluctuations leading to a better exploration of the configuration space.

The theoretical background of this biased MC technique is explicitly described in [29]. To adapt the cluster-MC approach to systems consisting of hard lenses, the closest surface distance for this geometry needs to be determined reliably with a fast method.

A. Closest surface distance of lenses

A lens is the section of two spheres with radius R_0 whose centers are less than $2R_0$ apart from each other. The generating spheres' radius R_0, depending on the equatorial radius r_{eq} and

*joachim.wagner@uni-rostock.de

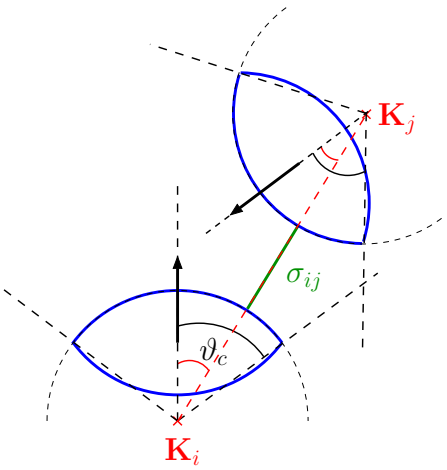

FIG. 1. Closest surface distance between undercritically inclined lenses. In this case (i) the closest surface distance is between the spherical caps of both lenses.

the aspect ratio ν, reads as

$$R_0 = \frac{1+\nu^2}{2\nu} r_{\mathrm{eq}}. \tag{1}$$

In principle, the presented algorithm to determine the closest surface distance σ_{ij} of lenses is an extension of the overlap algorithm of lenses in [21]. It assumes an overlap-free constellation of two lenses i and j with centers of mass $\mathbf{r}_i$ and $\mathbf{r}_j$ as well as orientations $\hat{\mathbf{u}}_i$ and $\hat{\mathbf{u}}_j$. The closest surface distance between two lenses can occur (i) between two spherical caps, (ii) between a spherical cap of one and the equatorial circle of the other lens, or (iii) between the equatorial circles of two lenses.

Let $\mathbf{K}_i$ and $\mathbf{K}_j$ be the centers of the most distant generating spheres and $\hat{\mathbf{u}}_\mathrm{s} = (\mathbf{K}_j - \mathbf{K}_i)/\|\mathbf{K}_j - \mathbf{K}_i\|$ the direction of their distance vector. Let us further define $\vartheta_\mathrm{c} = \arccos[(1-\nu^2)/(1+\nu^2)]$ as aperture of the critical cone. If the angles enclosed between the distance vector $\hat{\mathbf{u}}_s$ and both directors $\hat{\mathbf{u}}_i$ and $\hat{\mathbf{u}}_j$ are smaller than the critical angle ϑ_c, both lenses are undercritically inclined. In this case the closest surface distance is between two spherical caps and is given by

$$\sigma_{ij} = \|\mathbf{K}_j - \mathbf{K}_i\| - 2\,R_0 \tag{2}$$

as visualized in Fig. 1.

Otherwise at least one equatorial circle limits the closest surface distance. The point on the equator of lens j closest to $\mathbf{K}_i$ is

$$\mathbf{P}_j = \mathbf{r}_j + r_{\mathrm{eq}} \frac{\hat{\mathbf{u}}_j \times [(\mathbf{K}_i - \mathbf{r}_j) \times \hat{\mathbf{u}}_j]}{\|\hat{\mathbf{u}}_j \times [(\mathbf{K}_i - \mathbf{r}_j) \times \hat{\mathbf{u}}_j]\|}, \tag{3}$$

leading to the closest surface distance σ_{ij}

$$\sigma_{ij} = \|\mathbf{P}_j - \mathbf{K}_i\| - R_0 \tag{4}$$

under the condition

$$\frac{\mathbf{P}_j - \mathbf{K}_i}{\|\mathbf{P}_j - \mathbf{K}_i\|} \cdot \hat{\mathbf{u}}_i > \cos\vartheta_\mathrm{c}, \tag{5}$$

corresponding to case (ii). By interchanging the indices i and j in Eq. (3), Eq. (4) and the constraint Eq. (5), the closest surface distance between the equator of lens i and lens j is obtained (Fig. 2).

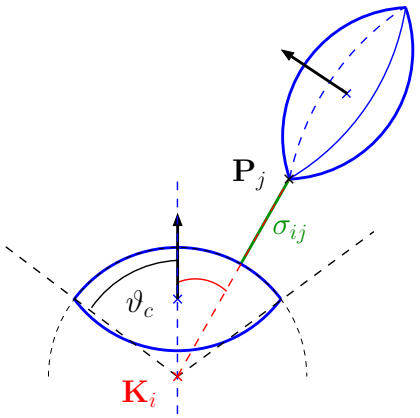

FIG. 2. Closest surface distance of critically inclined lenses case ii) fulfilling the constraint in Eq. (5). The closest surface distance occurs between the equator of one lens and the spherical cap of the other.

The remaining case (iii), i.e., the closest surface distance between both equators is illustrated in Fig. 3, where the constraint Eq. (5) is not fulfilled. The remaining problem is the closest distance between possibly incongruent circles in the three-dimensional space, which can be reliably determined using the algorithm of Vranek [30].

The described approach was validated by a numerical brute force routine using a parametrized surface and comparison to data computed by means of a standard (N, p, T) algorithm for different densities and aspect ratios.

B. Simulation details

Equation-of-state data for isotropic and nematic phases is calculated from compression simulations of systems typically with 1000 particles initialized from a cubic lattice with randomly aligned directors at a volume fraction of $\varphi = 0.05$. These are equilibrated for 10^6 steps and subsequently compressed to the pressure of interest. After an additional equilibration phase, a production run with 5×10^7 steps is performed. A step is hereby defined as N random particle displacement or rotation attempts and a single volume fluctuation attempt.

To determine the limits of the isotropic phase for aspect ratios that transition into a solid phase additional expansion simulations from dense monoclinic SM2 crystals containing between 972 and 1040 particles are performed. Here, addi-

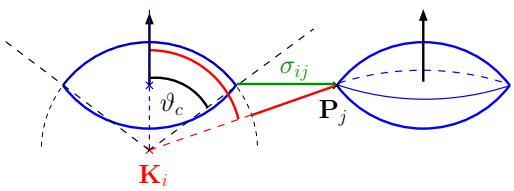

FIG. 3. Closest surface distance of critically inclined lenses case iii) which do not fulfill the constraint in Eq. (5). Here the closest surface distance lies between both equators and can be related to the closest distance between two possibly incongruent circles in the three-dimensional space.

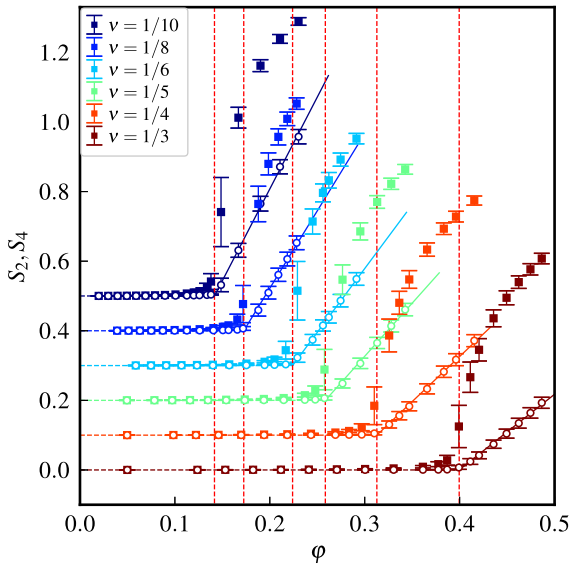

FIG. 4. Order parameters S_2 (closed squares) and S_4 (open circles) depending on the volume fraction φ for lenses of selected aspect ratios ν separated by arbitrary offsets. The vertical, dashed red lines represent the critical volume fractions φ_c determined by the roots of the linear increasing order parameters $S_4(\varphi)$ within the nematic phase.

tional shape fluctuations of the simulation box as described in [29] at constant volume are introduced whereby independent subsequent runs with at least 2×10^8 steps are performed.

The characteristic length δ steering the cluster formation probability is tuned during the second equilibration phase to obtain $N_b/N \approx 1/4$ where N_b is the number of created bonds. This guarantees percolation rejections to be less than 1 %, even for highly anisotropic particles.

III. RESULTS AND DISCUSSION

A. Phase boundaries in the hard-lens system

The aim of this work is the calculation of equation-of-state data in the isotropic phase of hard lenses. In the first step, the phase boundaries of the isotropic phase are determined. In analogy to oblate, hard ellipsoids of revolution, we expect transitions from the isotropic to nematic, plastic crystalline, and monoclinic crystalline phases. In the following, we map the phase diagram by evaluating characteristic observables.

The orientational correlation in nematic phases can be quantified by the nematic order parameters

$$S_2 = \left\langle \tfrac{1}{2}\left(3x_i^2 - 1\right)\right\rangle_{x_i} \tag{6}$$

and

$$S_4 = \left\langle \tfrac{1}{8}\left(35x_i^4 - 30x_i^2 + 3\right)\right\rangle_{x_i}. \tag{7}$$

To just identify the existence of nematic order, we use as previously described [29] the inner product $x_i = \hat{\mathbf{u}}_j.\hat{\mathbf{u}}_k$ of the particle orientations $\hat{\mathbf{u}}_j$ and $\hat{\mathbf{u}}_k$. To fulfill the minimum image convention, we again restrict the averages to the periodic boundary conditions. In Fig. 4, the order parameters S_2 and S_4 are displayed in dependence on the volume fraction φ. Since the increase of S_4 is more pronounced than that of S_2,

TABLE I. Phase boundaries for the isotropic phase of hard lenses.

ν	Phase Transition	φ_c	$\beta p_c r_{eq}^3$
1/10	I → N	0.142(2)	2.15(4)
1/8	I → N	0.173(2)	2.25(4)
1/6	I → N	0.224(2)	2.48(4)
1/5	I → N	0.258(2)	2.65(5)
1/4	I → N	0.313(2)	3.07(5)
1/3	I → N	0.400(2)	4.09(7)
1/2	I → SM2	0.555(3)	8.10(19)
2/3	I → PS	0.606(6)	7.9(4)
4/5	I → PS	0.505(6)	2.33(10)
10/11	I → PS	0.480(5)	1.54(7)

we extrapolate S_4 to its root to determine the critical volume fraction φ_c for the isotropic-nematic phase transition. The critical volume fractions φ_c and reduced coexistence pressures $\beta p_c r_{eq}^3$ are compiled in Table I.

In analogy to the phase behavior of oblate, hard ellipsoids of revolution, for aspect ratios $\nu \geqslant 1/2$ transitions into solid phases exist. To map the phase boundaries between the isotropic phase and the monoclinic crystalline SM2 phase, expansion simulations starting from dense SM2 crystals are performed. While for aspect ratio $\nu = 1/2$ a direct transition from the crystalline SM2 phase to the isotropic phase is observed, for $\nu \geqslant 2/3$, first a transition to a plastic solid phase occurs, followed finally at lower densities by the transition to the isotropic fluid phase. The reduced coexistence pressures and respective uncertainties are displayed in Fig. 5 depending on the volume fraction φ for different aspect ratios ν. The

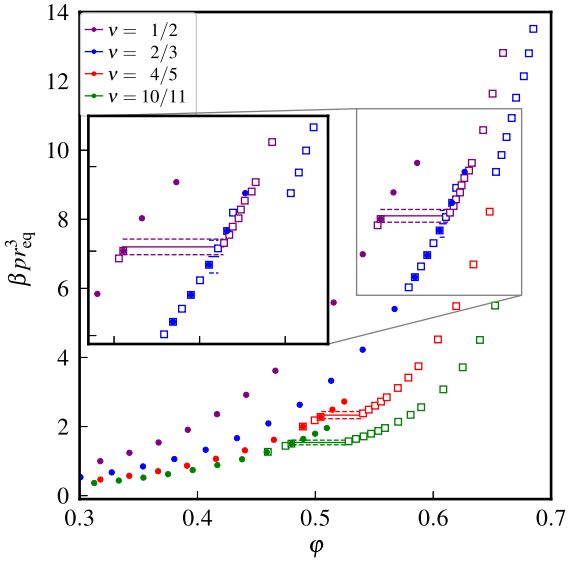

FIG. 5. Reduced pressure $\beta p r_{eq}^3$ depending on the volume fraction φ for hard lenses of selected aspect ratios ν. The closed circles represent data from compression simulations of the fluid phase, while open squares result from expansion simulations of solid monoclinic crystals. The horizontal solid lines represent the determined coexistence pressures with their uncertainties indicated by dashed horizontal lines.

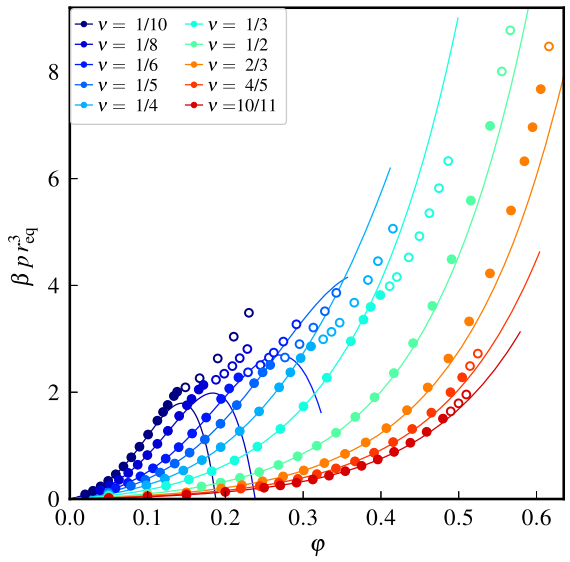

FIG. 6. Reduced pressure $\beta p r_{eq}^3$ depending on the volume fraction φ for hard lenses of selected aspect ratios ν. Closed circles represent equation-of-state data within the isotropic phase, while open circles display data beyond the phase transition. The solid lines represent the virial series using virial coefficients up to order eight from [21].

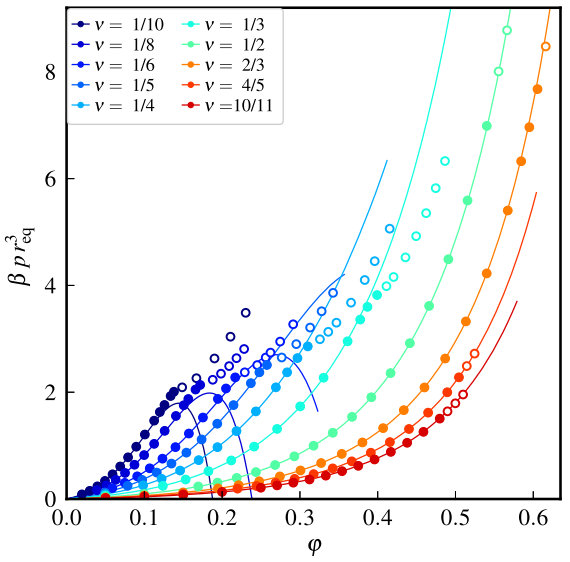

FIG. 7. Reduced pressure $\beta p r_{eq}^3$ depending on the volume fraction φ for hard lenses of selected aspect ratios ν. Closed circles represent equation-of-state data within the isotropic phase, while open circles display data beyond the phase transition. The solid lines represent the virial series up to order eight with a generalized Parsons-type truncation correction according to Eq. (11).

reduced coexistence pressures and critical volume fractions are additionally compiled in Table I.

B. Equation of state

Due to the absence of attractive interactions in the hard-lens system, the isotropic phase is supercritical and thus can be described using the virial approach

$$Z = \frac{p}{\varrho k_B T} = 1 + \sum_{i=2}^{\infty} B_i^* \varphi^{i-1} \tag{8}$$

in terms of the real gas factor Z. In this expansion in the volume fraction φ, the reduced virial coefficients B_i^* account for deviations from the ideal-gas equation of state. Here, the reduced virial coefficient B_i^* of order i accounts for real-gas effects induced by the formation of i-particle clusters.

As a first approach, we compare the simulation data, compiled in the Supplemental Material [31], with a virial approach using recently published hard-lens virial coefficients up to order $i = 8$ [21]. As displayed in Fig. 6, the initial departure from the ideal-gas behavior is excellently described for all aspect ratios in the low-density limit. Approaching the high-density limit of the isotropic phase, however, significant deviations can be observed when truncating the virial expansion for orders $i \geqslant 9$. This truncation even leads to unphysical, negative real gas factors for highly anisotropic particles.

Different approaches taking the contribution of so-far unknown, higher-order virial coefficients into account are discussed. Most of them are based on the Carnahan-Starling series [32] approximating the reduced virial coefficients of hard spheres as $B_i^* \approx i^2 + i - 2$. The reason why this approximation works surprisingly well for hard spheres is still not understood [33]. Inserting the Carnahan-Starling approximation in Eq. (8) leads to the closed expression

$$Z = \frac{1 + \varphi + \varphi^2 - \varphi^3}{(1-\varphi)^3} \tag{9}$$

for the real gas factor under the obvious constraint $\varphi < 1$. A common approach to correct for truncation effects is the use of all known virial coefficients up to order i_{max} for a given geometry and to approximate the contribution of the unknown ones by the complement of the Carnahan-Starling equation, where the factor $B_2^*/B_2^{*,HS}$ takes the specific shape into account. Here, B_2^* is the reduced, second virial coefficient of the respective geometry and $B_2^{*,HS} = 4$ is the reduced second virial coefficient of hard spheres [34,35]. This leads to the relation

$$Z = 1 + \sum_{i=2}^{i_{max}} B_i^* \varphi^{i-1} + \frac{B_2^*}{B_2^{*,HS}} \sum_{i=i_{max}+1}^{\infty} B_i^{*,HS} \varphi^{i-1} \tag{10}$$

for the real gas factor. In our case, using $i_{max} = 8$,

$$Z = 1 + \sum_{i=2}^{8} B_i^* \varphi^{i-1} + \frac{B_2^*}{4} \frac{2\varphi^8(35\varphi^2 - 78\varphi + 44)}{(1-\varphi)^3} \tag{11}$$

is obtained [29]. The solid lines in Fig. 7 represent the truncation-corrected equation of state Eq. (11). For moderately anisotropic lenses with aspect ratio $\nu \geqslant 1/5$ the simulation data are within the stability region of the isotropic phase indicated by closed symbols in good agreement to the suggested truncation correction. For higher anisotropic lenses, however, this correction fails. This is in accordance to the findings for oblate hard ellipsoids of revolution, where identically this correction works reasonably up to the same anisotropy parameter $\nu \geqslant 1/5$ as recently reported. This indicates that not the specific shape, but the extent of the short and long

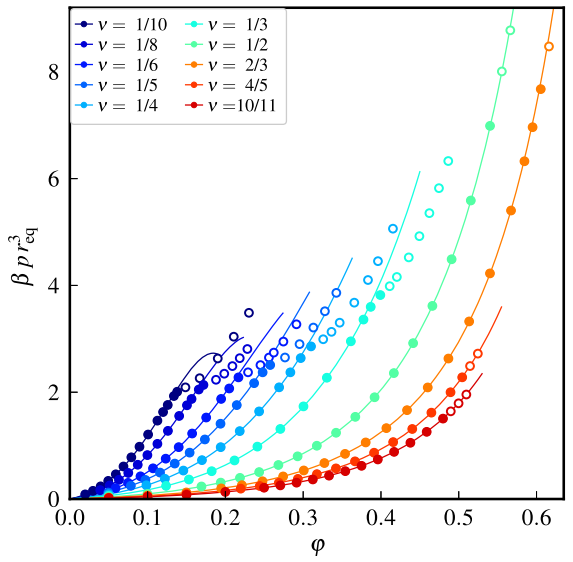

FIG. 8. Reduced pressure $\beta p r_{eq}^3$ depending on the volume fraction φ for selected aspect ratios of hard lenses. The solid lines represent least-squares fits of the proposed, generalized Carnahan-Starling equation of state [Eq. (12)] to the simulation data. Closed symbols represent equation-of-state data of the isotropic phase, while open symbols display data beyond the phase transition.

axes causes this effect and confirms our assumption that long-range orientational correlations not reflected by clusters of limited size, but intrinsically taken into account in simulations using several hundred particles are a plausible physical reason. The spatial extent of orientational correlations drastically increases for highly anisotropic particles and cannot be taken into account by the second virial coefficient B_2^* as a single shape-dependent correction factor: the second virial coefficient only reflects short-range orientational correlations in two-particle clusters. Here, the maximum interaction length, where the orientation plays a role, equals in the case of hard-body interaction the maximum contact distance, i.e., the particles largest extent.

To provide a simple, heuristic equation for the isotropic phase of hard lenses, we provide in analogy to hard, oblate ellipsoids of revolution, a generalized Carnahan-Starling approach, where the real gas factor Z reads as

$$Z = \frac{1 + \gamma_0\varphi + \gamma_1\varphi^2 - \gamma_2\varphi^3}{(1-\varphi)^3}. \tag{12}$$

Choosing the parameter $\gamma_0 = B_2^* - 3$, the virial expansion is asymptotically recovered in the low-density limit. Since the second virial coefficient B_2^* is analytically known for convex shapes, just two parameters γ_1 and γ_2 need to be determined from least-squares fits of simulation data in the isotropic phase employing Eq. (12). As visible in Fig. 8, the simulation data can be described excellently using this simple approach. The optimum parameters γ_1 and γ_2 are compiled in Table II depending on the aspect ratio ν.

C. Comparison with oblate ellipsoids

The dimensionless real gas factor Z is a quantity that describes the equation of state independent of topological

TABLE II. Optimum parameters γ_1 and γ_2 obtained from least-squares fits of the simulation data using the generalized Carnahan-Starling approach [Eq. (12)] depending on the aspect ratio ν. Additionally, the density limits of the data considered are indicated.

		Coefficients	
ν	Limits	γ_1	γ_2
1/10	$0.020 < \varphi < 0.142$	111.14681(13)	764.7883(13)
1/8	$0.039 < \varphi < 0.173$	67.73726(20)	382.6916(16)
1/6	$0.059 < \varphi < 0.224$	34.83358(16)	151.8094(10)
1/5	$0.049 < \varphi < 0.258$	21.57179(10)	77.6509(6)
1/4	$0.050 < \varphi < 0.313$	12.60231(9)	36.5776(4)
1/3	$0.050 < \varphi < 0.400$	6.17223(7)	13.15453(20)
1/2	$0.050 < \varphi < 0.555$	2.31013(13)	3.2334(4)
2/3	$0.050 < \varphi < 0.606$	1.45092(7)	1.75807(14)
4/5	$0.050 < \varphi < 0.505$	1.17826(10)	1.28442(25)
10/11	$0.050 < \varphi < 0.480$	1.07893(12)	1.1153(4)

parameters of the respective shape depending on the volume fraction φ. The comparison with our previously published data [29] shows that systematically at any volume fraction the real gas factor of lenses exceeds that of ellipsoids with the same aspect ratio (Fig. 9). Despite the shape of both oblate solids of revolution is quite similar, the detailed geometry has a significant impact on the equation of state already for moderately anisotropic particles. While at small anisotropies with $\nu \geqslant 4/5$ the real gas factors approximately coincide, already at $\nu = 1/2$ significant differences are observed. Even larger differences appear for aspect ratios where an isotropic-nematic phase transition occurs.

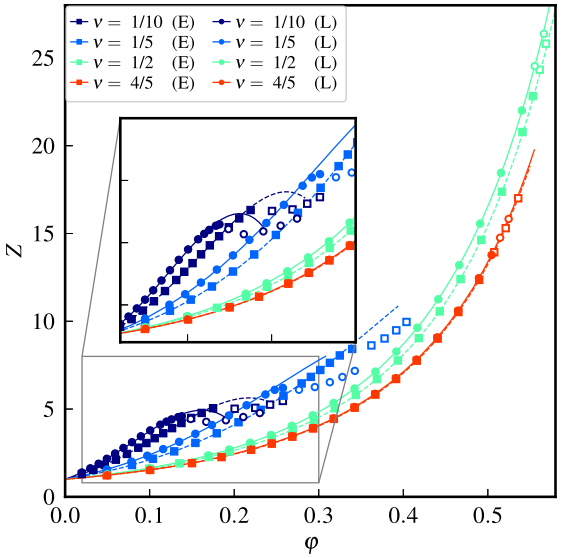

FIG. 9. Comparison of real gas factors Z for hard lenses and hard, oblate ellipsoids of revolution depending on the volume fraction φ for selected aspect ratios ν. The dashed lines with squares indicate data of ellipsoids, while that of lenses is displayed as circles with solid lines. Data for objects with the same aspect ratio are displayed with the same color. The data for ellipsoids are from [29].

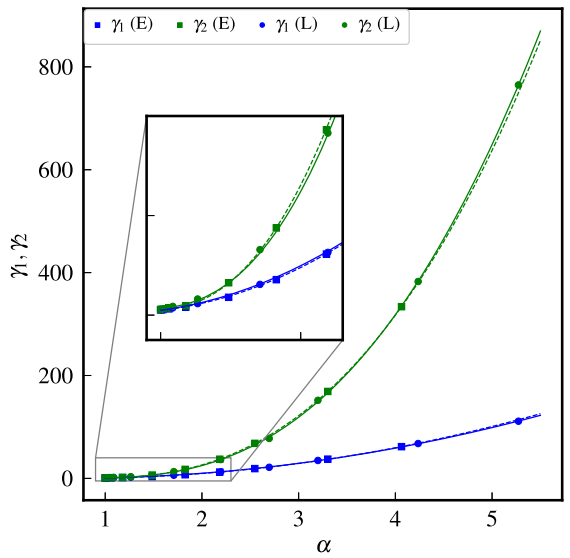

FIG. 10. Heuristic parameters γ_1 and γ_2 of the suggested, Carnahan-Starling type equation of state [Eq. (12)] depending on the excess part of the mutual excluded volume α [Eq. (13)]. Data of ellipsoids are displayed by dashed lines and squares, that of lenses by circles and solid lines.

This is in accordance to the orientationally averaged excluded volume equal to the second virial coefficient: The reduced second virial coefficient $B_2^* = B_2/V_\mathrm{P}$, i.e., the second virial coefficient normalized to the respective particle volume V_P, of lenses exceeds that of ellipsoids of revolution at the same aspect ratio ν. This is caused by the lenses' strongly increasing contribution of the equatorial singularity to the mean radius of curvature with rising anisometry [36]. As a further effect, a shift of the isotropic-nematic phase transition of lenses to lower critical volume fractions φ_c compared to oblate ellipsoids of revolution at the same aspect ratio ν is observed.

We have previously shown that reduced virial coefficients $\tilde{B}_i = B_i/B_2^{i-1}$ in first approximation show a universal behavior with respect to the rescaled excess part of the excluded volume, also known as nonsphericity parameter. The latter quantity is defined as

$$\alpha = \frac{B_2 - V_\mathrm{P}}{3V_\mathrm{P}} \tag{13}$$

with B_2 denoting the second virial coefficient and V_P the volume of the respective geometry. For both oblate shapes, the suggested generalized Carnahan-Starling relations with only two heuristic parameters γ_1 and γ_2 describe the equation-of-state data within the isotropic phase of both geometries surprisingly well.

Analyzing the dependence of both heuristic parameters on the rescaled excess part of the excluded volume α identically shows in first approximation a universal behavior, nearly independent on the specific particle shape (Fig. 10). This again indicates that the excess part of the mutual excluded volume is the essential quantity that determines the equation of state for oblate, hard solids of revolution. The solid and dashed lines as a guide to the eye are second-order polynomials in the case of γ_1 and fourth-order polynomials in the case of γ_2.

IV. SUMMARY AND OUTLOOK

As previously shown, cluster MC is an efficient method to calculate equation-of-state data of hard-body systems within the (N, p, T) ensemble with high accuracy and comparatively small numerical effort. The benefit of cluster MC increases especially in the case of anisotropic particles with the complexity of the overlap problem for the particle shape of interest. In addition to the contact problem, for cluster MC, however, at least an estimation for the closest surface distance is required.

We describe a method to exactly determine the closest surface distance for hard lenses based on our previously published contact algorithm [21]. Herewith, after tracing the phase boundaries of the isotropic phase of the hard-lens fluid, we calculated novel, precise equation-of-state data in the stability region of this phase. With access to equation-of-state data of both, hard, oblate ellipsoids of revolution and hard lenses, the influence of the detailed particle shape beyond the aspect ratio is analyzed.

The equation-of-state data for hard lenses is compared to a virial approach using recently published virial coefficients up to order eight and truncation effects, caused by so far unknown higher-order virial coefficients, are analyzed. For moderately anisotropic lenses with aspect ratio $\nu \geqslant 1/5$, a Parson-type correction is capable of reasonably describing the equation of state in the isotropic phase. Although this approach replaces unknown, higher virial coefficients by rescaled hard-sphere coefficients with a scaling factor taking only the second virial coefficient and thus two-particle interactions into account, the Parson correction is an excellent closure relation for moderately anisotropic particles within the isotropic phase. This correction, however, fails for highly anisotropic lenses as previously observed in the case of oblate, hard ellipsoids of revolution. As a heuristic approach, we suggest a generalized Carnahan-Starling ansatz with in addition to the analytically known second virial coeffiecient two adjustable parameters γ_1 and γ_2. This heuristic approach describes the equation of state within the isotropic phase surprisingly well despite its simplicity.

A significant shape dependence is observed for the real gas factor Z as a function of the volume fraction φ at identical aspect ratio ν. The parameters γ_1 and γ_2, however, show in first approximation for both oblate geometries a universal dependence on the rescaled excess part of the mutual excluded volume α. Hereby, a reliable interpolation for equation-of-state data for unknown aspect ratios is possible.

To gain further insights, if this seemingly universal behavior holds for different, possibly prolate geometries, additional equation-of-state data for such systems needs to be analyzed. Possible candidates could be prolate ellipsoids of revolution and spherocylinders, where the contact problem is already solved and differences in the phase behavior are known.

ACKNOWLEDGMENTS

P.M. gratefully acknowledges financial support by the Universität Rostock within the Ph.D. scholarship program.

[1] J. A. Barker and D. Henderson, Rev. Mod. Phys. **48**, 587 (1976).
[2] P. N. Pusey, *Colloidal Suspensions in Liquids, Freezing and Glass Transition* (Elsevier, 1991), pp. 765–942.
[3] S. Sacanna and D. J. Pine, Curr. Opin. Colloid Interface Sci. **16**, 96 (2011).
[4] M. J. Solomon, Curr. Opin. Colloid Interface Sci. **16**, 158 (2011).
[5] P. Tierno, Phys. Chem. Chem. Phys. **16**, 23515 (2014).
[6] P.-G. de Gennes, Rev. Mod. Phys. **71**, S374 (1999).
[7] I. Muševič, Materials **11**, 24 (2017).
[8] I. I. Smalyukh, Annu. Rev. Condens. Matter Phys. **9**, 207 (2018).
[9] D. Frenkel, B. M. Mulder, and J. P. McTague, Phys. Rev. Lett. **52**, 287 (1984).
[10] P. Bolhuis and D. Frenkel, J. Chem. Phys. **106**, 666 (1997).
[11] D. van der Beek and H. N. W. Lekkerkerker, Langmuir **20**, 8582 (2004).
[12] I. Nezbeda, Chem. Phys. Lett. **41**, 55 (1976).
[13] T. Boublík, Mol. Phys. **42**, 209 (1981).
[14] T. Boublík and I. Nezbeda, Collect. Czech. Chem. Commun. **51**, 2301 (1986).
[15] Y. Song and E. A. Mason, Phys. Rev. A **41**, 3121 (1990).
[16] Y. Singh, Phys. Rep. **207**, 351 (1991).
[17] A. Isihara, J. Chem. Phys. **18**, 1446 (1950).
[18] A. Isihara and T. Hayashida, J. Phys. Soc. Jpn. **6**, 40 (1951).
[19] H. Hadwiger, Experientia **7**, 395 (1951).
[20] T. Boublík, Mol. Phys. **27**, 1415 (1974).
[21] P. Marienhagen, R. Hellmann, and J. Wagner, Phys. Rev. E **104**, 015308 (2021).
[22] G. Odriozola, J. Chem. Phys. **136**, 134505 (2012).
[23] G. Bautista-Carbajal, A. Moncho-Jordá, and G. Odriozola, J. Chem. Phys. **138**, 064501 (2013).
[24] G. Cinacchi and S. Torquato, J. Chem. Phys. **143**, 224506 (2015).
[25] G. Cinacchi and S. Torquato, Soft Matter **14**, 8205 (2018).
[26] G. Cinacchi and S. Torquato, Phys. Rev. E **100**, 062902 (2019).
[27] N. G. Almarza, J. Chem. Phys. **130**, 184106 (2009).
[28] N. Tasios and M. Dijkstra, J. Chem. Phys. **146**, 144901 (2017).
[29] P. Marienhagen and J. Wagner, Phys. Rev. E **105**, 014125 (2022).
[30] D. Vranek, J. Graph. Tools **7**, 23 (2002).
[31] See Supplemental Material at http://link.aps.org/supplemental/10.1103/PhysRevE.106.014101 for the determined equation-of-state data of hard lenses.
[32] N. F. Carnahan and K. E. Starling, J. Chem. Phys. **51**, 635 (1969).
[33] Y. Song, E. A. Mason, and R. M. Stratt, J. Phys. Chem. **93**, 6916 (1989).
[34] J. D. Parsons, Phys. Rev. A **19**, 1225 (1979).
[35] C. Vega, Mol. Phys. **92**, 651 (1997).
[36] E. Herold, R. Hellmann, and J. Wagner, J. Chem. Phys. **147**, 204102 (2017).